THE JOURNAL OF PHYSICAL CHEMISTRY C

Article

pubs.acs.org/JPCC

Pyroelectrocatalytic Disinfection Using the Pyroelectric Effect of Nano- and Microcrystalline $LiNbO_3$ and $LiTaO_3$ Particles

Emanuel Gutmann,*[,†,‡] Annegret Benke,[§] Katharina Gerth,[§] Horst Böttcher,[#] Erik Mehner,[†] Christin Klein,[∥] Udo Krause-Buchholz,[⊥] Ute Bergmann,[§] Wolfgang Pompe,[§] and Dirk C. Meyer[†]

[†]Institute of Experimental Physics, TU Bergakademie Freiberg, Leipziger Strasse 23, D-09596 Freiberg, Germany

[‡]Department Photonics and Sensorics, Gesellschaft zur Förderung von Medizin-, Bio- und Umwelttechnologien e.V. (GMBU), Felsbachstrasse 7, D-07745 Jena, Germany

[§]Institute of Materials Science and Max Bergmann Center of Biomaterials, [∥]Institute of Structural Physics, [⊥]Institute of Genetics, TU Dresden, D-01062 Dresden, Germany

[#]Department Functional Coatings, Gesellschaft zur Förderung von Medizin-, Bio- und Umwelttechnologien e.V. (GMBU), Postfach 520165, D-01317 Dresden, Germany

ABSTRACT: $LiNbO_3$ (LN) and $LiTaO_3$ (LT) materials of polar crystal structure exhibit a spontaneous polarization that can be changed by temperature. This phenomenon, commonly known as the pyroelectric effect, leads to the generation of surface charges that in turn are the source for a pyroelectrocatalytic or pyroelectrochemical activity of these materials described in this paper. It can also be regarded as a selective conversion of thermal via electrical to chemical energy based on the pyroelectric effect. In this context, we have investigated the impact of thermally excited pyroelectric LN and LT nano- and microcrystalline powder materials on the bacterium *Escherichia coli* in aqueous solutions. Powders have been prepared both by milling of commercially available single crystals and by precursor-based solution routes. Our results show that in dependence on the crystallite size and surface area of the pyroelectric particulate material in direct contact with the cells and/or their culture solution, a high antimicrobial activity can be achieved. On the basis of further experimental results of oxidative conversion of the fluorescent dye 2′,7′-dichlorofluorescin, a disinfection mechanism including the formation of reactive oxygen species at the pyroelectric particle surface is proposed. The phenomenon is discussed in analogy to the well-established photocatalytic disinfection mechanism.

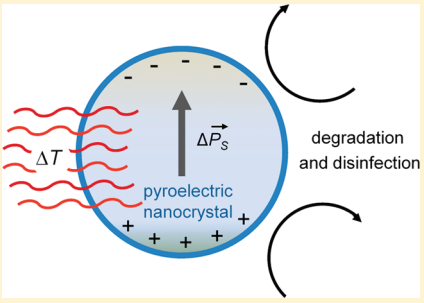

INTRODUCTION

In recent years the demand for environmentally friendly physical disinfection methods has considerably risen, since on the one hand (waste) water treatment, air purification, self-sterilization, and infection prevention have gained more and more importance and on the other hand an increasing awareness of climate and environment protection has evolved in the global community. In this context, several advanced oxidation processes like UV or photocatalytic disinfection methods—with the latter using oxide semiconductors such as TiO_2 under illumination—are already in the state of technological application in most of the aforementioned fields.[1−5] Photoexcited TiO_2-based catalysts are able to form reactive oxygen species (ROS) (e.g., hydroxyl radicals by reaction of the photoexited holes with water, $h^+ + H_2O \rightarrow {}^\bullet OH + H^+$, and hydroperoxide radicals by reaction of photoelectrons with oxygen, $e^- + O_2 + H^+ \rightarrow {}^\bullet OOH$) which can mineralize most organic materials and destroy living microorganisms.[6] Another comparably new approach is based on high (pulsed) electric fields (on the order of 40 kV/cm) that irreversibly perforate the cell membrane and thus destroy a microorganism.[7,8] Hereby the electrodes are arranged outside the reaction chamber in order to avoid ionic compensation as well as electrochemical reactions that would considerably reduce the resulting electric field strength. A low-energy thermally activated disinfection method, as introduced in this paper, has some benefits or could at least be a useful complement to photoactivated or pulsed electric field based methods, since one could effectively use residual heat from numerous processes and also operate in the dark.

It is well-known that a heterogeneous catalytic reaction can be promoted by several approaches altering the electrostatic conditions at the catalyst surface, including long-range electrostatic fields.[9−11] On the other hand, the overpotential of an electrochemical reaction can be reduced by appropriate modification of the electrochemically active electrode surface, which is commonly known as electrocatalysis. It is also worth recalling that a heterogeneous catalytic system, where an electrified interphase is formed by the charge transfer from the catalyst to the reacting phase, has to be considered as an electrochemical system, too.[12] In the light of this, a material with electrochemical or catalytic properties that can be

Received: November 7, 2011
Revised: January 25, 2012
Published: February 7, 2012

activated or altered by an intrinsically developed surface potential evoked by external excitation would be of great interest.

One possibility of generating a charged surface is to apply a mechanical stress to a piezoelectric material. It was shown recently that following this approach an electrostatic potential large enough to facilitate electrolysis of water molecules can develop even in liquid phase.[13] Applying ultrasonic vibration to piezoelectric, substrate-supported, fibrous ZnO and dendritic $BaTiO_3$ materials generated H_2 and O_2 in stoichiometric ratio. The authors have termed this phenomenon the piezoelectrochemical effect. Since it converts mechanical energy directly into chemical energy, it may have a huge potential for application in future energy-scavenging technology, especially by generating "clean" hydrogen.[14]

An alternative approach to generate a surface charge based on the bulk photovoltaic effect has been reported.[15] Thereby irradiation of donor-doped $LiNbO_3$ (LN) crystals with photons of sub-band-gap, donor-adapted energy results in an asymmetric charge carrier generation and subsequent formation of oppositely charged surfaces due to charge carrier transport and accumulation. Dipolar fields with field strengths up to 100 kV/cm that are able to irreversibly perforate the membrane of living cells can develop. The authors used this effect to effectively kill tumor cells in vitro.

Besides the piezoelectric and bulk photovoltaic effect, the pyroelectric effect can also be addressed to generate a charged surface. Hereby a surface charge $\sigma = \Delta P_s$ (with the spontaneous polarization P_s) develops in response to a temperature change ΔT. LN and $LiTaO_3$ (LT) are ferroelectric materials that beside piezoelectric and photorefractive properties also show a pronounced pyroelectric behavior.[16] Compared to other commonly used pyroelectrics, like triglycine sulfate, barium titanate, and lead-based titanates or germanates, the combination of several material properties and technological aspects makes LN and LT favorable for application in environmental technology. They are widely available, nontoxic, and insoluble in water, and their polarization is highly stable, even in unidirectional poled materials at the nanometer scale. For the pyroelectric coefficient $p = dP_s/dT$, different values ranging from -85 to -50 $\mu C/m^2$ K (LN) and -230 to -176 $\mu C/m^2$ K (LT) are reported in the literature.[17−19] Traditional applications in nonlinear optics and in surface acoustic wave technology are solely based on the bulk properties of LN and LT.[20,21] However, in the last few years their microscopic surface properties, including chemical redox activity, came into the scientific focus. As an example, the substrate-assisted self-assembly of nanostructures, taking advantage of different redox characteristics at oppositely poled crystal faces or surface domains, was intensively investigated.[22,23] Several follow up studies were conducted, focusing on understanding the geometric and electronic structure as well as adsorption properties of LN surfaces.[24−31] Also the influence of the polarization direction of a supporting ferroelectric substrate on the (photo)catalytic activity of deposited metal clusters and thin metal or TiO_2 films has been investigated.[32−35] In contrast to the influence of the (static) polarization direction on surface chemistry, only very few investigations have been carried out concerning the influence of (transient) variation of the polarization magnitude as for example induced by the pyroelectric effect. In this context, temperature programmed desorption experiments revealed an effect of the LN polarity on the thermal desorption of various polar molecules, which was attributed to electrostatic interactions of the polar molecules with uncompensated pyroelectric surface charges.[28,29] Under equilibrium conditions the bound polarization charges at the surface of a pyroelectric material are screened by (mobile) compensation charges that can either be intrinsic charge carriers (e^-, h^+, charged defects) or extrinsic ionic charges.[36] A temperature rise results in a decrease of polarization magnitude and thus temporarily in an imbalance between decreasing bound polarization charges and at the surface remaining screening charges. This effect is employed in various thermal and infrared sensing applications whereby the pyroelectric potential is converted to a current signal via electrical contacts at opposite surfaces of the pyroelectric component.[37,38] When the surface is left bare, especially under aqueous conditions, the net charges generated during temperature changes should at least be partly available for redox reactions with molecular species. Furthermore, temporarily huge electrostatic potentials can develop, large enough to provide the necessary activation energy or redox potential to induce a catalytic or electrochemical reaction.[14] When the ionic screening charge availability and mobility in the environment are reduced, e.g., in (diluted) gas atmosphere, the electrostatic field strength becomes large enough to induce direct field ionization of molecular species. This effect is already used for various technological applications, including electron, ion, X-ray, and even neutron emission.[39−43]

In this study, we report on the antibacterial and oxidative properties of pyroelectric LN and LT nano- and microcrystalline particles that are thermally excited around ambient temperature. To the best of our knowledge, this represents the discovery of a new phenomenon—briefly termed the pyroelectrocatalytic effect—that anchors in the generation of pyroelectric surface charges and subsequent transfer to adsorbed molecular species at the pyroelectric material surface. It further represents a (pyroelectrochemical) conversion of thermal energy to chemical energy offering an enormous potential in energy-scavenging application based on the conversion of residual heat and naturally or artificially provided temperature variations. Since the efficiency of the pyroelectrocatalytic effect—in direct analogy to classical heterogeneous catalytic, photocatalytic, or electrochemical processes—is expected to scale with the active surface area, several routes for the preparation of micro- and nanocrystalline LN and LT powder materials are tested. The materials structural, morphological, antibacterial, and oxidative properties are investigated, comprehensively discussed, and finally summarized in a proposal of the underlying microscopic mechanism.

EXPERIMENTAL METHODS

Preparation of LN and LT Powder Material. Micro- and nanocrystalline LN and LT powders were prepared both by milling of commercially available single crystals (sc) and by different precursor-based solution routes. For LN-sc and LT-sc powder samples, single crystals of LN and LT (supplied by CrysTec) were crushed by hand with a corundum mortar and pestle and afterward high-energy ball milled using a vibration mill (Pulverisette 0, Fritsch) with corundum mortar and a single corundum ball of 50 mm in diameter. The weight ratio of powder to ball was about 1:25. Milling was conducted in air atmosphere and the vibration amplitude was set to 2.5 mm. Depending on the initial weight and mean crystal size in the fragmented single crystal material after crushing, milling times of 6 h and more were necessary to obtain a powder of solely

dx.doi.org/10.1021/jp210686m | J. Phys. Chem. C 2012, 116, 5383−5393

sub-millimeter-sized particles that could be used for fractionation. Three different fractions of LT and LN single crystal powder with nominal particle sizes of <5, 5−10, and 10−15 μm were gained by wet sieving the as-milled powder with distilled water using a vibration siever (Analysette 3, Fritsch) equipped with Ni microsieves of different mesh sizes. The aqueous powder suspensions were heated on a hot plate at moderate temperature for several hours until complete vaporization of water. The remaining powders were used without further drying.

For solution preparation of LN powder materials three routes and for LT powder materials two routes were tested using different niobium and tantalum precursors, respectively (see Table 1 for comparison). All used chemicals were supplied by Sigma-Aldrich and employed without further purification. For LN-1, 2.66 g (0.01 mol) of Nb_2O_5 , 1.32 g (0.02 mol) of LiAc, and 60 mL of glacial acetic acid were refluxed for 6 h. After vaporization of the solvent, the solid material was annealed at a temperature of 600 °C for 2 h. The same route was applied for LT-1, except that the Nb_2O_5 precursor was replaced by 4.42 g (0.01 mol) of Ta_2O_5. For LN-2 a route after Wang et al.[44] was chosen, where 0.66 g (0.01 mol) of LiAc in 10 mL of water was mixed under stirring with 2.7 g (0.01 mol) of $NbCl_5$ in 30 mL of H_2O_2 (30%) and 6.3 g (0.03 mol) of citric acid. The mixture was heated up to 80 °C and the formed viscous gel was dried at 60 °C for 15 h. Afterward, the dried material was annealed at 600 °C for 5 h. The same route was applied for LT-2, except that the $NbCl_5$ precursor was replaced by 3.58 g (0.01 mol) of $TaCl_5$. The powder LN-3 was prepared by mixing 0.66 g (0.01 mol) of LiAc in 10 mL of acetic acid (50%) with 3.03 g (0.01 mol) of ammonium niobate oxalate $[(NH_4)NbO(C_2O_4)\cdot H_2O]$ in 30 mL of water and refluxing for 6 h. The obtained precipitation was annealed at 600 °C for 2 h. In order to increase the active surface area after the final annealing process, all five solution-prepared granular materials were ball milled under the same conditions as the single crystal material but for a shorter duration of only 30 min. The powder to ball weight ratio was on the order of 1:250. From solution-prepared materials only powder fractions of nominal particle size <5 μm, which were analogous to the single crystal powders obtained by wet sieving and vaporization of water, were used for further experiments.

Table 1. Summary of LN and LT Powder Samples and Preparation Conditions

powder sample	description [niobium/tantalum precursor]
LN-sc (<5 μm)	LN, from single crystal, milled and fractioned
LN-sc (5−10 μm)	LN, from single crystal, milled and fractioned
LN-sc (10−15 μm)	LN, from single crystal, milled and fractioned
LN-1	LN, solution route 1 [Nb_2O_5], milled and fractioned to <5 μm
LN-2	LN, solution route 2 [$NbCl_5$], milled and fractioned to <5 μm
LN-3	LN, solution route 3 [$(NH_4)NbO(C_2O_5)_2\cdot H_2O$],
LT-sc (<5 μm)	LT, from single crystal, milled and fractioned
LT-sc (5−10 μm)	LT, from single crystal, milled and fractioned
LT-sc (10−15 μm)	LT, from single crystal, milled and fractioned
LT-1	LT, solution route 1 [Ta_2O_5], milled and fractioned to <5 μm
LT-2	LT, solution route 2 [$TaCl_5$], milled and fractioned to <5 μm

Structural and Morphological Characterization. The crystalline powder materials were characterized using X-ray diffraction (XRD) and Rietveld analysis of the obtained diffraction patterns. The patterns were recorded in Bragg-Brentano geometry using Cu Kα radiation with an X-ray diffractometer D8 (Bruker AXS) equipped with a secondary graphite (003) monochromator and scintillation detector. In order to identify the crystalline phases present in the samples, the PDF-2[45] and ICSD[46] databases were used. The crystal structures of as-identified and in the Rietveld analysis applied phases of LN, $LiNb_3O_8$, Nb_2O_5, LT, Ta_2O_5, α-Al_2O_3 were derived from refs 47, 48, 49, 50, 51, and 52, respectively. The Rietveld analysis was performed using the program TOPAS[53] in order to determine the mean crystallite sizes and specific mass fractions of the phases present in the samples. X-ray emission profile and instrumental parameters of the diffraction experiment were determined beforehand by analyzing the diffraction pattern of a silicon standard powder (NIST SRM 640c). The reflection profiles in the diffraction patterns were analyzed using a fundamental parameters approach convolution algorithm that includes the refinement of the full width at half-maximum of a Gaussian profile to account for sample-induced diffraction line broadening.[54] Compensating texture effects with spherical harmonics was necessary for almost all samples, excluding LN-1. Furthermore, the refinement model employed a third-order polynomial background curve and isotropic Debye−Waller factors. Strain or microstrain was not taken into account since it yielded unrealistic high strain values and mean crystallite sizes contradicting the particle sizes estimated from scanning electron microscopy (SEM) measurements. Converged refinement of these models resulted in R_{wp} and goodness-of-fit values ranging from 9.2 to 15.25% and 1.08 to 1.27, respectively. Since serial correlation effects of parameters refined during Rietveld analysis cannot be excluded, the standard deviations of the mean crystallite size and mass fractions of target and impurity phases were corrected using the program RIET-ESD[55] based on the algorithm given by Berar and Lelann.[56]

The powder sample morphology was investigated by SEM using a DSM 982 Gemini electron microscope (Zeiss). The dry crystal powder samples were mounted on carbon pads and carbon-coated before insertion into the microscope. For the electrons an acceleration voltage of 5 kV was set at the cathode.

Antimicrobial Activity against *Escherichia coli*. For all experiments *E. coli* DSM 498 (ATCC 23716) was cultivated aerobically in nutrient yeast broth (NY) at 37 °C while being shook on a rotating platform at 100 rpm for 30 h.

Different LN and LT powder materials were weighed and placed into a reaction tube (1.5 mL) to which 150 μL of a 30-h-old *E. coli* culture was added. The final concentration of powder was 0.3 g mL^{-1}.

For LN and LT powder material from the solution route, causing a pH value above pH 9.5, a 30-h-old *E. coli* culture was centrifuged. The supernatant was removed, and the cells were washed three times with 0.15 M Tris/HCl buffer pH 7.7 and filled up with 150 μL buffer to obtain the initial powder concentration. To investigate the influence of buffer on antibacterial activity, the same procedure was applied for powder samples from single crystal material LT-sc (<5 μm). pH values of the samples were estimated using standard litmus paper (Macherey-Nagel).

Disinfection experiments were carried out in a Thermoshaker (Thermomixer comfort, Eppendorf) with cyclic alternating

dx.doi.org/10.1021/jp210686m | J. Phys. Chem. C 2012, 116, 5383−5393

temperatures between 20 and 45 °C for 6 h maximum and shaking at 600 rpm for mixtures of LN or LT powder and *E. coli* cells. The $T(t)$ curve of the thermal treatment was measured with a Cu/CuNi thermocouple (tolerance 0.5 °C) directly placed into the reaction tube. The shape of one temperature cycle is shown in Figure 1. The overall duration of one temperature cycle was 32 min within which the sample was kept at a temperature of 45 °C for 10 min. The quantification of vital cells was carried out by fluorescent staining with LIVE/DEAD BacLight (Invitrogen) and cell counting using a fluorescence microscope (Axiovert 200M, Zeiss). Red fluorescence indicates cells that are considered to be dead or dying, whereas cells with an intact membrane are stained green. The relative error of the portion of vital cells was estimated according to the standard deviation of three independent experiments performed with two identical samples and cell counting of three image sections each. The cultivation was monitored by recording growth curves and fluorescent staining. Both have shown that in the period between 30 and 40 h (where the disinfection experiments were performed) the cultivation was in the log phase and the portion of vital cells was above 95%.

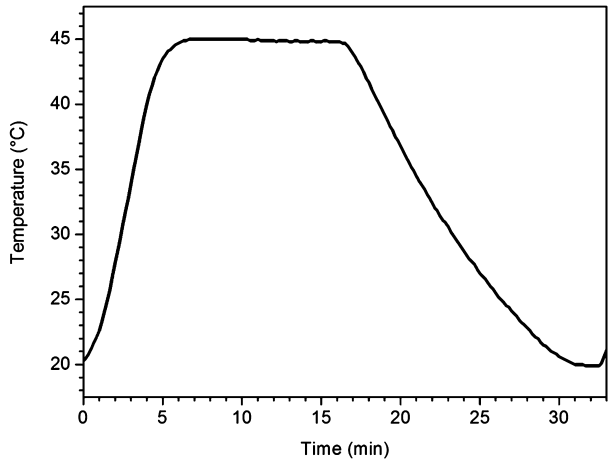

Figure 1. Temperature curve of one cycle of the thermal treatment as preset in the thermoshaker for disinfection experiments and ROS-induced oxidation of DCFH.

ROS-Induced Oxidation of 2′,7′-Dichlorodihydrofluorescin (DCFH). To investigate the pyroelectric induced formation of ROS in aqueous solutions, the indicator dye DCFH was used.[57,58] It is oxidized to the highly fluorescent molecule 2′,7′-dichlorofluorescin (DCF) by ROS. The fluorescence intensities correlate with the concentration of ROS.

2′,7′-Dichlorodihydrofluorescin diacetate (DCFH-DA, Sigma-Aldrich) was dissolved in ethanol as stock solution and subsequently diluted in double distilled water to a concentration of 0.24 mM. The deesterification of DCFH-DA to DCFH proceeds in basic milieu.[57,59] As mentioned above, the pH of solutions containing either LN or LT crystal powder is shifted toward basic pH and hence triggers complete conversion to DCFH. For each sample, 10 mg of LN or LT powder was resuspended in 120 μL of double distilled water, and 30 μL of 0.24 mM DCFH-DA was added. The samples were heated from 20 to 45 °C and then cooled to 20 °C in a thermoshaker (Thermomixer comfort, Eppendorf) at a heating and cooling rate of 5 K/min. For details of the thermal treatment, see the previous subsection and Figure 1. In intervals of 3 min, the samples were mixed with 600 rpm for a period of 9 s. This procedure was repeated for 6 cycles. Finally, the samples were centrifuged (8000*g*, 6 min) and the fluorescence intensity of the supernatants was measured with a fluorospectrometer (Nanodrop ND 3300, ThermoScientific) at wavelengths of 470 and 521 nm for excitation and emission, respectively. The relative error of DCF fluorescence intensity was estimated according to the standard deviation of a series of 10 identical samples of LN-sc (<5 μm) with triplicate measurements each.

RESULTS

Structural and Morphological Properties of LN and LT Powders. As can be seen from the SEM images in Figure 2, as-prepared powder fractions LN-sc (<5 μm) and LT-sc (<5 μm) are characterized by a similar morphology. Larger micrometer-sized particles with sharp edges are agglomerated with smaller nanometer-sized particles. In LT-sc (<5 μm) many more nanometer-sized particles are present, which points to a more effective milling procedure of LT compared to LN single crystals. Particles from solution routes show a spongelike morphology consisting of agglomerated nanometer-sized and more or less spherical particles. In contrast to all other samples from solution routes, the powder LN-1 (Figure 2c; LT-1 is

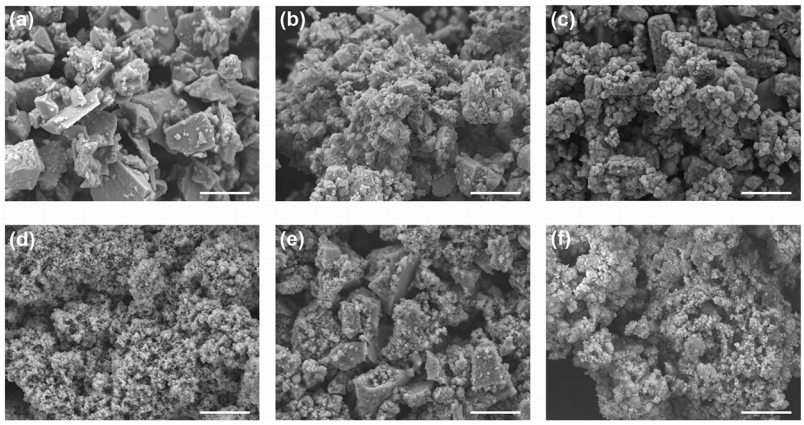

Figure 2. SEM pictures of LN and LT powder fractions <5 μm. Samples a and b are prepared by milling of single crystals (a, LN-sc; b, LT-sc) and samples c–f are prepared by solution routes (c, LN-1; d, LN-2; e, LN-3; f, LT-2). See Table 1 for a comparison of preparation parameters.

dx.doi.org/10.1021/jp210686m | *J. Phys. Chem. C* 2012, 116, 5383–5393

similar, though not shown in the figure) is characterized by micrometer-sized relatively dense agglomerates of particles with sizes in the range of 100−400 nm. Also some micrometer-sized particles with a smooth surface can be identified, which might represent impurity phases (see XRD results in Figure 2 and Table 2 for comparison). The powders LN-2 and LT-2 (Figure 2d,f) from $NbCl_5$- and $TaCl_5$-based solution routes, respectively, exhibit fine particles that form large and nanoporous agglomerates. Furthermore, on closer examination of Figure 2f, beside the fine particles also some platelike particles can be seen. These particles most likely correspond to the α-Al_2O_3 phase, as observed in the diffraction patterns (see below). The SEM image of LN-3 (Figure 2e) shows an overall similar morphology to that of the powders prepared from single crystals, but the micrometer-sized particles show a high degree of nanoporosity.

Table 2. Phase Content and Mean Crystallite Size of LN and LT Powder Samples According to Rietveld Analysis of Measured XRD Patterns

powder sample	mean crystallite size LN, LT (nm)	mass fraction LN, LT (wt %)	mass fraction of impurity phase (wt %)
LN-sc (<5 μm)	295.1 ± 3.3	100.0 ± 3.2	
LN-1	89.8 ± 0.7	85.1 ± 3.5	5.6 ± 0.5 ($LiNb_3O_8$) 9.3 ± 0.7 (Nb_2O_5)
LN-2	69.7 ± 0.6	100.0 ± 3.1	
LN-3	67.2 ± 0.6	98.5 ± 2.6	1.5 ± 0.1 ($LiNb_3O_8$)
LT-sc (<5 μm)	307.2 ± 3.3	100.0 ± 3.5	
LT-1	59.9 ± 0.5	83.3 ± 2.7	16.7 ± 0.5 (Ta_2O_5)
LT-2	33.8 ± 0.3	57.5 ± 1.9	42.5 ± 0.3 (α-Al_2O_3)

Table 2 summarizes the results for the mean crystallite sizes and specific phase content according to the quantitative analysis of XRD patterns. Corresponding experimental and Rietveld refinement calculated diffraction patterns are compared in Figure 3. Both powders from single crystal LN-sc and LT-sc (<5 μm) consist solely of crystalline LN and LT, respectively, with a mean crystallite size of about 300 nm. The according diffraction patterns show sharp and intense reflections, whereas for all samples from solution routes, much broader reflections occur in the patterns, pointing to much smaller sizes of crystallites. For the mean crystallite size of solution prepared powders values below 100 nm are obtained from Rietveld refinement. Both powders LN-1 and LT-1 from Nb_2O_5 and Ta_2O_5 precursor based solutions exhibit a comparatively high fraction of about 15 wt % of Nb-rich and Ta-rich impurity phases, respectively. The powder gained from $NbCl_5$ precursor based solution LN-2 is phase pure LN with a mean crystallite size of about 70 nm. In the analogously prepared powder LT-2 (precursor $TaCl_5$), beside the target phase LT a large fraction of α-Al_2O_3 (42.5 wt %) was detected. This can be attributed to abrasion of the corundum ball during the ball milling process. A similar effect was recently observed by Wilkening et al., which used an alumina shaker mill for high-energy ball milling of commercial LT powder.[60] It is assumable that this effect can be diminished by choosing a higher powder to ball weight ratio and smaller vibration amplitudes, but for reasons of comparability of preparation conditions, we decided not to vary these parameters in our experiments. In the powder LN-3, beside the target phase LN a small fraction of $LiNb_3O_8$ (1.5 wt %) was identified.

Antimicrobial Activity of Thermally Excited LN and LT Powders. To test a potential antimicrobial activity of pyroelectric crystallites, *E. coli*, a common bacteria of humans often causing sepsis, was chosen. Bacterial cells of untreated samples of a 30 h culture showed an almost exclusive green fluorescence, documenting that the majority of bacterial cells is alive (Figure 4a). However, the portion of red fluorescent cells, indicating dead cells, increase strongly after 2 h of thermal cycling in the presence of LT-sc (5−10 μm) and more pronounced already after 1 h treatment with LT-sc (<5 μm) as active pyroelectric crystallites (Figure 4b,c). Quantification of the lethality rate in dependency on the crystallite type and size revealed the strong impact of the particle size used (Figure 5−7). While particles of either LN or LT larger than 10 μm possessed no effect on cell vitality, the lethality increased dramatically with decreasing the particle size smaller than 5 μm. This indicates that the antibacterial effect strongly depends on the nominal particle size, i.e. a high surface area of fine powders. Comparing the portion of dead cells after treatment for 1 h with <5 μm particles of either LN or LT revealed a slightly better disinfective strength for LT (above 95% dead cells) than for LN (~80% dead cells). Replacement of culture media by Tris/HCl buffer pH 7.7 did not significantly influence the disinfection rate (Figures 5 and 6).

All powders from solution routes are characterized by a high antimicrobial activity against *E. coli*, too (Figure 7). Nevertheless, in Figure 7 we only display values measured with powders LN-1, LT-1, and LT-2. The antimicrobial activity of the powder LT-2 is less severe compared to the other two samples. This can be attributed to the high fraction (42.5 wt %) of (pyroelectrocatalytic inactive) α-Al_2O_3 in this sample. The powders LN-2 and LN-3 also yielded a high rate of disinfection, but already after 1.5 h the pH in these samples reached values of nearly 10 despite buffering. In this case, a strong antimicrobial effect from solution pH on *E. coli* cannot be excluded (see also Discussion).

ROS-Induced Oxidation of DCFH Facilitated by Thermally Excited LN and LT Powders. The formation of ROS in water by pyroelectric powder materials subjected to thermal excitation was indirectly measured using the redox-sensitive indicator DCFH, which is converted to a fluorescent dye upon oxidation by ROS (Figure 8).[57,58] Control samples without crystals are devoid of fluorescence. In contrast, pyroelectric particles are capable of inducing fluorescence to a different extent when thermically activated. In line with the results of the bacterial viability test, we find a dependency of the fluorescence intensity of DCF on the particle size of the pyroelectric single crystal powder. Particles of either LN or LT smaller than 5 μm possess the highest activity, possibly by providing a large surface area for reaction. Unexpected, samples of LN-sc (5−10 μm) are less active than samples with the largest particle size. This can possibly be attributed to the presence of a high fraction of agglomerates composed of smaller particles, which might have also been retained by the 10 μm sieve (see also Discussion). Surprisingly, fluorescence dramatically increased by a factor of 10−100 in the presence of powder from the solution routes. Samples from solution route 1 (based on Nb_2O_5 or Ta_2O_5) showed lower fluorescence intensities than samples from solution routes 2 or 3 [based on $NbCl_5$ and $TaCl_5$ or $(NH_4)NbO(C_2O_4)_2{\cdot}H_2O$].

dx.doi.org/10.1021/jp210686m | J. Phys. Chem. C 2012, 116, 5383−5393

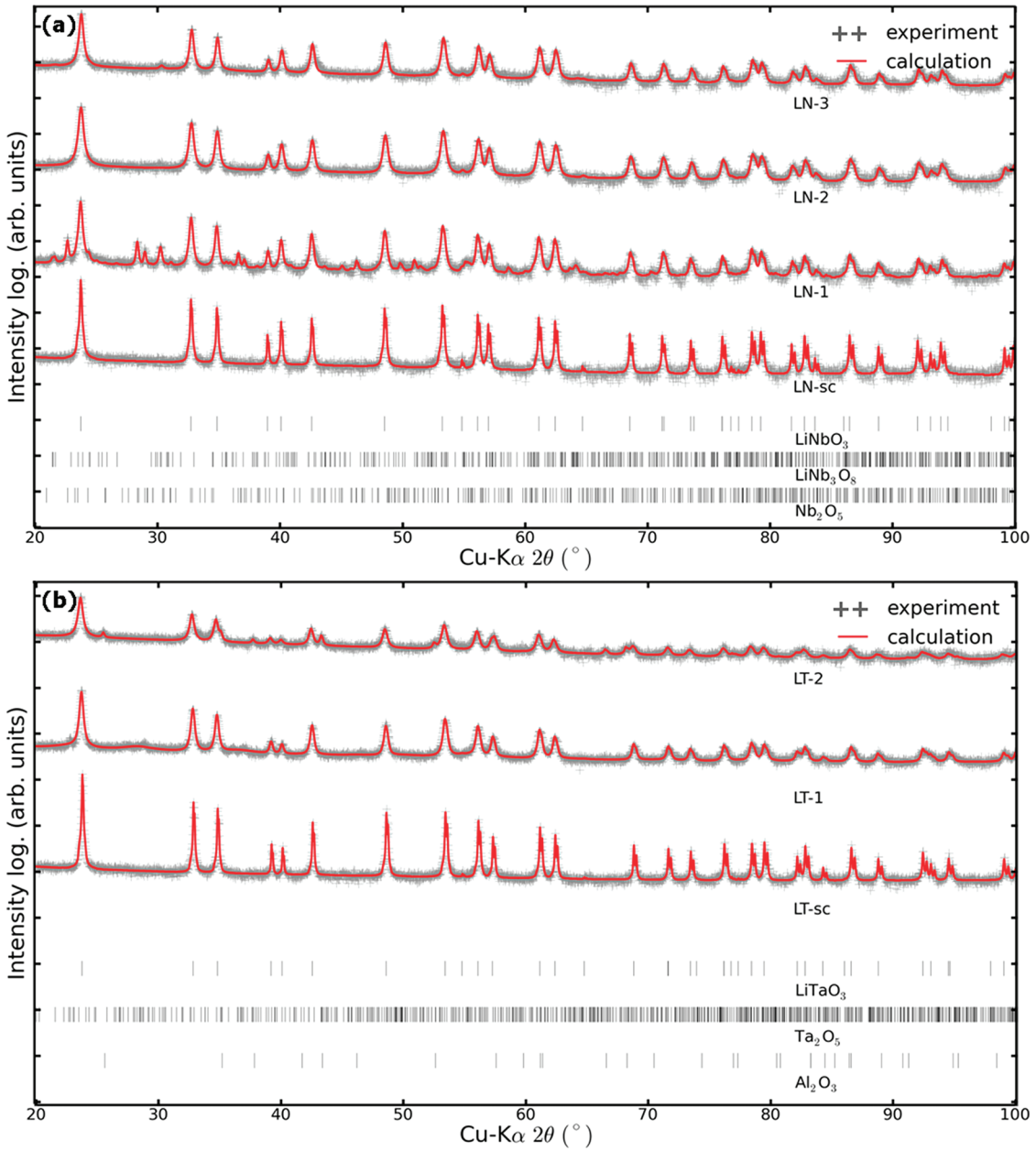

Figure 3. Quantitative XRD analysis of (a) LN and (b) LT powder samples. Parameters of the best fit models obtained by Rietveld refinement (calculated diffraction patterns are represented by red solid lines) are given in Table 2.

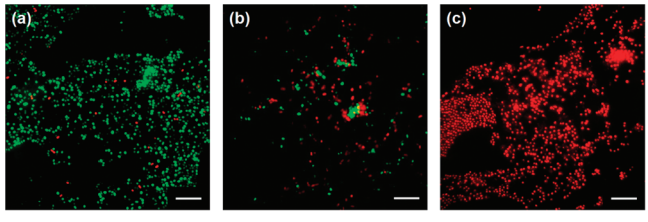

Figure 4. Vitality staining of bacterial cultures. Fluorescence microscopy images of LIVE/DEAD stains of *E. coli* cultures not subjected to thermal treatment (a), after thermal treatment for 2 h in the presence of LT-sc (5−10 μm) (b), and following 1 h thermal treatment in the presence of LT-sc (<5 μm) (c).

DISCUSSION

Influence of Temperature and pH of Aqueous Solution on *E. coli* Culture Vitality. Temperature and pH are important environmental factors influencing the growth and vitality of organisms. Thus, test conditions of disinfection experiments were configured in a manner that cell death as a result of temperature or pH can be excluded. In fact, the results of disinfection experiments in Figures 4−6 document disinfection due to the pyroelectric effect. *E. coli* bacteria are mesophilic organisms with optimal growth temperatures between 20 and 45 °C and a range of tolerance of 8−48 °C.[61] Therefore, excitation of pyroelectric crystals by temperature alterations has been carried out in the physiological range between 20 and 45 °C. It has been shown that an antibacterial effect of the pyroelectric crystal powder is realized only upon temperature variation. Parallel experiments with analogous

dx.doi.org/10.1021/jp210686m | J. Phys. Chem. C 2012, 116, 5383−5393

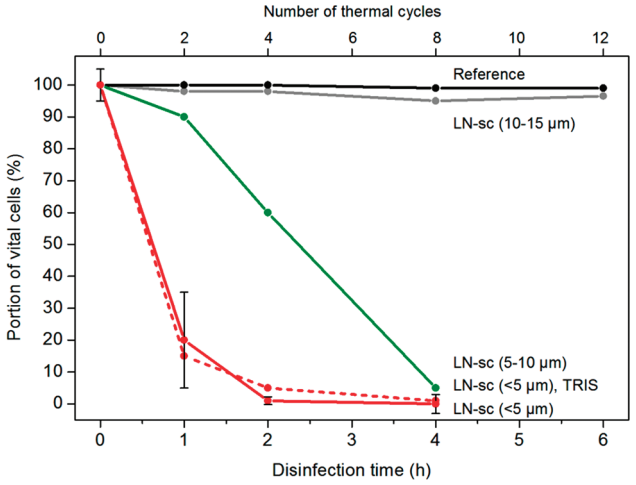

Figure 5. Antibacterial activity of LN powder of different particle sizes from single crystal (see Table 1) against *E. coli*. Samples with culture medium (continuous lines) and Tris/HCl pH 7.7 buffer (dotted lines) are compared. As reference, a sample with *E. coli* in culture medium but without LN powder was subjected to cyclic thermal excitation and shaking. Error bars are estimated according to the standard deviation and for reasons of clarity given for one representative data series only.

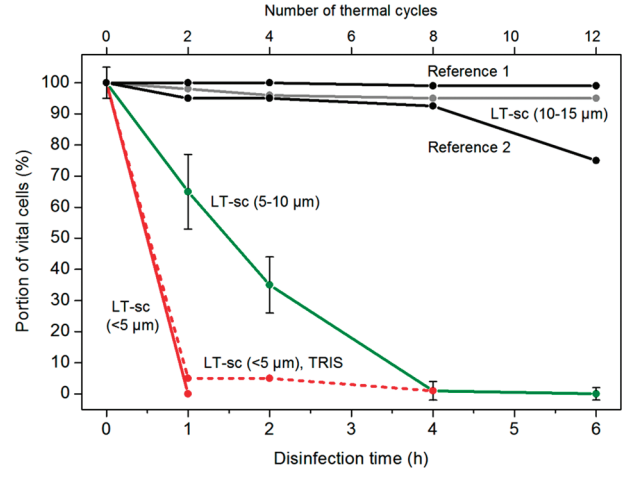

Figure 6. Antibacterial activity of LT powders of different particle sizes from single crystal (see also Table 1) against *E. coli*. Samples with culture medium (continuous lines) and Tris/HCl pH 7.7 buffer (dotted lines) are compared. As reference 1 a sample with *E. coli* in culture medium but without LT powder was subjected to cyclic thermal excitation and shaking. Reference 2 represents an *E. coli* culture sample with LT-sc (<5 μm) powder but without thermal excitation. Error bars are estimated according to the standard deviation and for reasons of clarity given for one representative data series only.

samples kept at constant temperature revealed only marginal disinfection effects. It should be noted that minimal temperature changes (±0.5 °C) during the experimental period due to the device specific accuracy of temperature regulation cannot be obviated. Furthermore, against this background a possible antimicrobial effect due to Li^+ ion leaching seems to be implausible. Since the leaching rate of Li^+ ions is expected not to vary significantly with the slight temperature rise of 25 K, it cannot account for the large difference in disinfection rate of thermally excited powder samples and reference powder samples without thermal excitation.

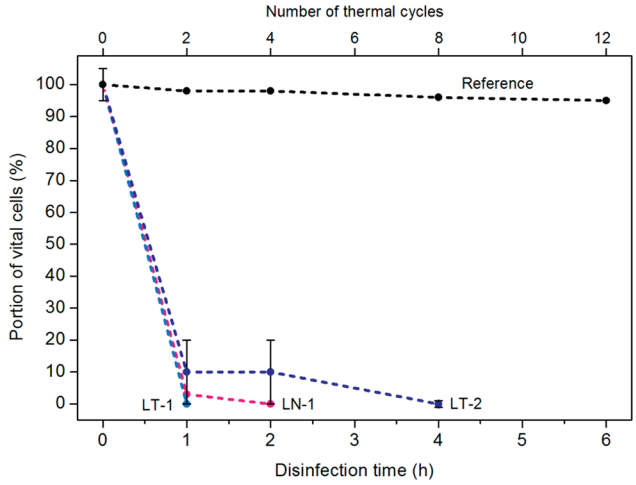

Figure 7. Antibacterial activity of LN and LT powders from different solution routes (see Table 1 for comparison) against *E. coli*. To all samples with powders from solution routes (dotted lines) a Tris/HCl pH 7.7 buffer was added. As reference a sample with *E. coli* also buffered in Tris but without LN or LT powder was subjected to cyclic thermal excitation and shaking. Error bars are estimated according to the standard deviation and for reasons of clarity given for one representative data series only.

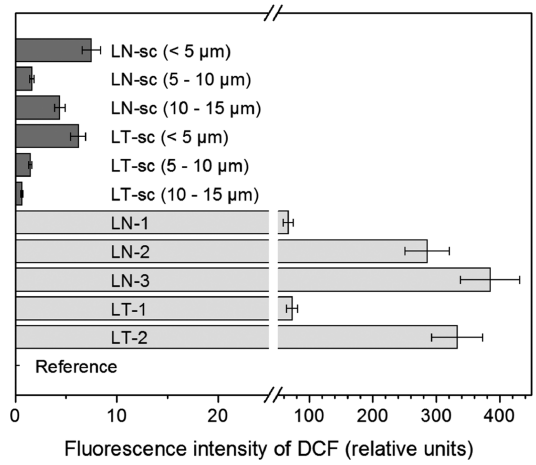

Figure 8. Fluorescence intensity of DCF after cyclic thermal excitation of pyroelectric particles. Aqueous solution of DCFH containing LN or LT powders from both single crystals (LN-sc, LT-sc) and solution routes (LN-1 to LT-2; see Table 1 for comparison) were thermally treated. As reference, a dye solution without powder was subjected to cyclic thermal excitation. Error bars represent the relative standard deviations as estimated from a series of 10 identical samples LN-sc (<5 μm) and three measurements each.

In the literature some reports on the influence of pyroelectric particles on properties of aqueous solutions, such as pH value, can be found.[62,63] pH shifts toward alkaline range are described, but the underlying mechanisms are not really understood. In our experiments, similar pH shifts were observed. For this reason the pH influence on *E. coli* culture vitality has to be taken into account as well. In its natural habitat *E. coli* is exposed to different pH conditions with strong fluctuations. It grows over a wide range of pH values (pH 4.4−9.2), and its own metabolism shifts the external pH toward either extreme, depending on available nutrients and electron acceptors.[64] In spite of this wide range of tolerance, in our experiments cell death in consequence of pH was excluded by analyzing samples

dx.doi.org/10.1021/jp210686m | J. Phys. Chem. C 2012, 116, 5383−5393

in both culture medium and Tris/HCl buffer pH 7.7 for pH stabilization. No obvious differences were observed for powders prepared from single crystals in the corresponding disinfection experiments in buffered and unbuffered samples. Samples from solution route prepared particles had strong effects on the pH of the medium. Hence, all samples were buffered to maintain the pH below 9.5 and exclude the influence of extreme pH on the mortality rate. However, even in the presence of buffer, the pH of solutions with powders LN-2 and LN-3 rose to nearly pH 10. In this case, a strong antimicrobial effect from solution pH on *E. coli* cannot be excluded.

Influence of Powder Morphology and Phase Content on Antibacterial Activity against *E. coli* and Oxidation of DCFH. After ruling out an antibacterial effect solely due to pH change or temperature, a comparison of the particle activity regarding their morphological and structural properties was performed. An antibacterial effect due to the mechanical impact of the powder particles appears to be unlikely, since some of the pyroelectric powders do not significantly influence the *E. coli* vitality [see Figures 5 and 6, LN-sc (10−15 μm) and LT-sc (10−15 μm)]. Strikingly, our data on the mortality of *E. coli* and the fluorescence induction of DCFH document that, with smaller particle size and respectively larger surface area of powders from single crystals, both the antibacterial activity and rate of DCFH oxidation increase. The relative sizes of molecular or biological targets and the different LN and LT powder materials may also have some impact. The *E. coli* bacterium has a rodlike shape with dimensions of about 1 μm × 3 μm, whereas the size of a DCF molecule is approximately 1 nm. Thus, beside an increase in (pyroelectrocatalytically active) surface area, also the similar dimensions of crystal particles or agglomerates and *E. coli* bacteria might positively effect the antibacterial activity of the pyroelectric powder with smaller nominal particle size.[65] Since both powder materials are equally prepared and characterized by similar morphologies, there is no significant difference between LN and LT materials of the same nominal particle size. Nevertheless, the slightly higher antibacterial activity of LT-sc powders (see Figures 5 and 6 for comparison) might either be attributed to the slightly higher pyroelectric coefficient or to the qualitatively higher fraction of small-sized particles present in the powder LT-sc compared to LN-sc (see SEM images in Figure 2a,b). However, SEM is only a local probe; i.e. it may not represent the particle size distribution of the entire fraction, especially since the mean crystallite sizes according to XRD (being an integral probe; see Table 2) are almost equal for both powders LT-sc and LN-sc (<5 μm). In the DCFH oxidation experiments (Figure 8) within the series of powders from single crystals the sample LN-sc (5−10 μm) is out of place. As discussed before, a possible explanation for this can be that a high fraction of particle agglomerates individually smaller than 10 μm might have been retained by the 10 μm sieve.

Compared to powder material from single crystals, thermal excitation of powders from solution routes resulted in both a higher rate of DCFH oxidation and a higher antibacterial activity; i.e., already after the first two thermal cycles 100% (with respect to detection accuracy) of bacteria were killed. Only the less severe antimicrobial activity of the powder LT-2 is an exception, but as discussed before, this can be attributed to the high fraction of (pyroelectrocatalytically inactive) α-Al_2O_3 present in this sample. All powders from solution routes, characterized by small crystallite and particle sizes (as well as a certain degree of porosity), are expected to yield a much larger surface area per weighted sample than powders from single crystals. In the disinfection experiments (Figures 5−7) the difference between powders from solution routes and powders from single crystals (<5 μm), especially LT-sc (<5 μm), is less pronounced than in the DCFH oxidation experiments (Figure 8). This is partly due to the experimental parameters chosen for disinfection; i.e., for a better differentiation shorter cycle durations and even smaller temperature intervals should be applied. It is expected that with powders from solution routes a strong antibacterial effect (100% of bacteria killed) is obtained already after a few minutes. Within the series of powders from solution routes the rate of DCFH oxidation is the smallest for the powders prepared from Nb_2O_5 or Ta_2O_5 precursors. The large difference cannot be solely attributed to their high fraction of impurity phase(s) but rather to their tendency to form large and relatively dense agglomerates, lowering the surface area (see Figure 2c). In aggregated systems also a compensation of surface charge due to contact of oppositely poled particle surfaces may account for lowering the rate of DCFH oxidation.

Proposed Mechanism of Pyroelectrocatalytic Disinfection and DCFH Oxidation. From the above discussion, further relying on theoretical considerations of an immediate screening of electrostatic fields by ionic species especially in aqueous conditions, a mechanism of pyroelectrocatalytic disinfection based on the impact of long-range electrostatic fields can be ruled out.[66] The increase in antibacterial activity and rate of DCFH oxidation with decreasing particle size clearly points to a mechanism where an intimate contact between pyroelectrocatalytically active powder and target molecule or bacterium is provided. For the mechanism of *E. coli* disinfection, beside well-known ROS-induced disruption or damaging of various cell functions or structures, also a dielectric permeabilization of the cell membrane can be responsible for cell death. The latter mechanism presupposes that the pyroelectric particle and bacterium are in intimate contact and the electrostatic field perforates the cell membrane, causing cell death.[15] For DCFH oxidation the situation is more explicit. Since the conversion of the indicator dye is facilitated by the oxidative action of ROS, a mechanism including the generation of surface adsorbed ROS has to be assumed. This mechanism does not conflict with the findings of Blázquez-Castro et al., which ruled out that ROS are responsible for cell death during their experiments.[15] Unfortunately, they conducted the ROS experiment only with a single crystal sample and not with the microcrystalline powder. Furthermore, their single crystal was an *X*-cut plate, thus exposing only a small fraction of polar compensated *Z*-cut side faces, which we mainly account for ROS formation in pyroelectrocatalytic disinfection. However, since the mechanisms of excitation are dissimilar, also the mechanisms of disinfection might be different. A major difference is, for example, that with the bulk photovoltaic effect intrinsic charge carriers from the crystal interior accumulate at the surface, whereas during the pyroelectrocatalytic effect the potential develops due to uncompensated extrinsic screening charge carriers located at the outer surface, respectively inner Helmholtz plane. In the latter case, charge transfer to adsorbed molecular species from the electrolyte might be facilitated.

In the following, a quantitative estimate of the charge generated at the surface of a pyroelectric crystal should be given, before the microscopic mechanism of the pyroelectrocatalytic effect is discussed. Neglecting compensation, a temperature change of ΔT = 10 K results in a charge density at

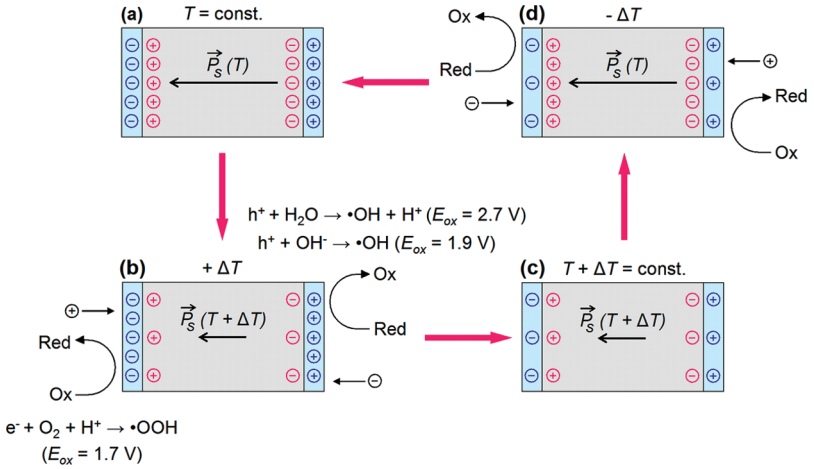

Figure 9. Scheme of a pyroelectrocatalytic cycle, i.e., thermal excitation of a pyroelectric crystal in aqueous conditions and subsequent surface reaction. In panels a and c the equilibrium situation at different temperatures is depicted, whereas panels b and d illustrate the situation of a surface potential development due to a transient imbalance between polarization (red circles) and screening charges (blue circles). If the surface potential in panels b and d exceeds the oxidation potentials (in b the oxidation potentials for hydroxyl radical[67] and hydroperoxide radical formation[68] are given as example), surface-adsorbed molecular species can undergo redox reactions, resulting in formation of ROS. A competing mechanism of charge compensation is the adsorption of ionic species from the electrolyte (black circles).

the LN(0001) surface of $\sigma = \Delta P_s = p\Delta T = 850\ \mu C/m^2$. The surface charge Q_s on one of the two (0001) surfaces of a cylindrical LN single crystal with 15 mm diameter and 5 mm thickness can be estimated from $Q_s = \Delta P_s A = 0.15\ \mu C$. With the unit charge e and the Avogadro constant N_A this corresponds to an amount of substance of 10^{-12} mol. A complete extrinsic compensation of this charge quantity would already be achieved by charge transfer to less than $^1/_{10}$ of a monolayer of surface adsorbed molecules.[27] Thus with macroscopic single crystals no significant electrochemical amount of substance conversion can be realized. However, increasing the surface area by milling the same single crystal to a powder with nanometer-sized crystals of cylindrical shape (50 nm diameter and 50 nm thickness) results in a surface charge of 15 C (one side). This corresponds to an amount of substance of 0.1 mol, which in liquid phase is equivalent to an electrochemical volume conversion in the milliliter range.

Considering a pyroelectric crystal in thermodynamic equilibrium with a surrounding electrolyte, the bound polarization charges are completely screened by compensation charge carriers (Figure 9a). Charge compensation is accompanied by a surface layer with corresponding electronic surface states. In the case of good insulators, such as LN and LT, this layer is mainly composed of surface chemisorbed, extrinsic chemical species, such as OH^- and the like.[66] In consequence of a pyroelectric excitation by means of temperature variation, the equilibrium is disturbed and a net surface charge develops (Figure 9b). These charges are located in electronic surface states. Surface-bound radical species similar to that generated by trapping of photoexited charge carriers during photocatalysis are likely to develop.[4] In the following the system strives to reduce the surface potential. This can be realized by charge transfer between chemisorbed surface species with adsorbed molecules from the surrounding electrolyte. A prerequisite for such a charge transfer is that the surface potential exceeds the standard redox potential of the redox couple involved. Otherwise, the chemical driving force (Gibbs' free energy) is below the threshold energy for the electrochemical reaction.[14] From an electronic point of view, charge transfer results in filling up or emptying electronic surface states occupied by screening charge carriers. A competing process to charge transfer is the adsorption of ionic species from the electrolyte, lowering the pyroelectrocatalytic efficiency of a material (see Figure 9b,d).[62]

CONCLUSIONS

We have reported on the disinfection properties of pyroelectric LN and LT powder materials under cyclical thermal excitation. Powders were prepared both by milling of commercially available single crystals and by precursor-based solution routes, with the latter yielding smaller crystallite and particle sizes, as observed by means of XRD and SEM. Results of *E. coli* disinfection show that, depending on the crystallite size and surface area of the pyroelectric particulate material in direct contact with the cells or their culture solution, a high antimicrobial activity can be achieved. It has been discussed that under the experimental conditions chosen an antimicrobial effect due to temperature and solution pH should be marginal, thus pointing to a pyroelectrocatalytic activity of the pyroelectric powder material when thermally excited. Further experimental results concerning the oxidative conversion of nonfluorescent DCFH to the fluorescent DCF suggest that the generation of ROS at the pyroelectric particle surface may account for the antimicrobial activity. Since the underlying phenomenon, briefly termed as the pyroelectrocatalytic effect, can be regarded as a conversion of thermal via electrical to chemical energy (and especially the formation of ROS), it should offer a huge potential not only in disinfection technology but also for degradation of organic matter or catalytic conversion for energy and environment application.

AUTHOR INFORMATION

Corresponding Author

*Tel. +49-3641-366710. Fax +49-3641-366777. E-mail: gutmann@gmbu.de.

Notes

The authors declare no competing financial interest.

■ ACKNOWLEDGMENTS

For fruitful and inspiring discussions we owe many thanks to Prof. Gerhard Roewer (Institut für Anorganische Chemie, TU Bergakademie Freiberg), Prof. Sven Kureti (Department of Energy Process Engineering and Chemical Engineering, TU Bergakademie Freiberg), Dr. Theo Woike (Institut für Strukturphysik, TU Dresden), and Benjamin Schulze (Laboratory of Organic and Macromolecular Chemistry, FSU Jena). Financial support by the German BMBF within the Framework "ForMaT" is gratefully acknowledged.

■ REFERENCES

(1) Oppenländer, T. *Photochemical Purification of Water an Air*; Wiley-VCH: Weinheim, 2003.
(2) Kühn, K. P.; Chaberny, I. F.; Massholder, K.; Stickler, M.; Benz, V. W.; Sonntag, H.-G.; Erdinger, L. *Chemosphere* **2003**, *53*, 71.
(3) Chong, M. N.; Jin, B.; Chow, C. W. K.; Saint, C. *Water Res.* **2010**, *44*, 2997.
(4) Chen, C.; Ma, W.; Zhao, J. *Chem. Soc. Rev.* **2010**, *39*, 4206.
(5) Zhang, D.; Li, G.; Yu, J. C. *J. Mater. Chem.* **2010**, *20*, 4529.
(6) Chen, X.; Mao, S. S. *Chem. Rev. (Washington, DC, U. S.)* **2007**, *107*, 2891.
(7) Heinz, V.; Alvarez, I.; Angersbach, A.; Knorr, D. *Trend Food Sci. Technol.* **2002**, *12*, 103.
(8) Lee, C.; Kim, J.; Yoon, J. *Chemosphere* **2011**, *82*, 1135.
(9) Vayenas, C. G.; Koutsodontis, C. G. *J. Chem. Phys.* **2008**, *128*, 182506.
(10) Pacchioni, G.; Lomas, J. R.; Illas, F. *J. Mol. Catal. A: Chem.* **1997**, *119*, 263.
(11) Kruse, N.; de Bocarmé, T. V. In *Handbook of Heterogeneous Catalysis*; Ertl, G., Knözinger, H., Schüth, F., Weitkamp, J., Eds.; Wiley-VCH: Weinheim, 2008; Vol. 2, pp 870−895.
(12) Horváth, I. T., Ed. *Encyclopedia of Catalysis*; Wiley Interscience: Hoboken, NJ, 2003; Vol. 3, pp 115−138.
(13) Hong, K.-S.; Xu, H.; Konishi, H.; Li, X. *J. Phys. Chem. Lett.* **2010**, *1*, 997.
(14) Xu, H.; Hong, K.-S.; Li, X. US Patent Application US 2010/0012479 A1, 2010.
(15) Blázquez-Castro, A.; Stockert, J. C.; López-Arias, B.; Juarranz, A.; Agulló-López, F.; García-Cabañes, A.; Carrascosa, M. *Photochem. Photobiol. Sci.* **2011**, *10*, 956.
(16) Lines, M. E.; Glass, A. M. *Principles and Applications of Ferroelectrics and Related Materials*; Clarendon Press: Oxford, 1977.
(17) Weis, R. S.; Gaylord, T. K. *Appl. Phys. A: Mater. Sci. Process.* **1985**, *37*, 191.
(18) Bhalla, A. S.; Liu, S. T. In *Landolt-Börnstein— Group III Condensed Matter*; Nelson, D. F., Ed.; Springer: Berlin, 1993; Vol. *29b*.
(19) Adachi, M.; Akishige, Y.; Asahi, T.; Deguchi, K.; Gesi, K.; Hasebe, K.; Hikita, T.; Ikeda, T.; Iwata, Y.; Komukae, M.; Mitsui, T.; Nakamura, E.; Nakatani, N.; Okuyama, M.; Osaka, T.; Sakai, A.; Sawaguchi, E.; Shiozaki, Y.; Takenaka, T.; Toyoda, K.; Tsukamoto, T.; Yagi, T. In *Landolt-Börnstein—Group III Condensed Matter*; Shiozaki, Y., Nakamura, E., Mitsui, T., Eds.; Springer: Berlin, 1993; Vol. *36A1*.
(20) Xu, Y. *Ferroelectric Materials and Their Applications*; Elsevier: Amsterdam, 1991.
(21) Volk, T.; Wöhlecke, M. *Lithium Niobate: Defects, Photorefraction and Ferroelectric Switching*; Springer: Berlin, 2008.
(22) Kalinin, S. V.; Bonnell, D. A.; Alvarez, T.; Lei, X.; Hu, Z.; Ferris, J. H.; Zhang, Q.; Dunn, S. *Nano Lett.* **2002**, *2*, 589.
(23) Tiwari, D.; Dunn, S. *J. Mater. Sci.* **2009**, *44*, 5063.
(24) Yun, Y.; Li, M.; Liao, D.; Kampschulte, L.; Altman, E. I. *Surf. Sci.* **2007**, *601*, 4636.
(25) Sanna, S.; Schmidt, W. G. *Phys. Rev. B* **2010**, *81*, 214116.
(26) Levchenko, S. V.; Rappe, A. M. *Phys. Rev. Lett.* **2008**, *100*, 256101.
(27) Yun, Y.; Kampschulte, L.; Li, M.; Liao, D.; Altman, E. I. *J. Phys. Chem. C* **2007**, *111*, 13951.
(28) Yun, Y.; Altman, E. I. *J. Am. Chem. Soc.* **2007**, *129*, 15684.
(29) Garra, J.; Vohs, J. M.; Bonnell, D. A. *Surf. Sci.* **2009**, *603*, 1106.
(30) Yang, W.-C.; Rodriguez, B. J.; Gruverman, A.; Nemanich, R. J. *J.Phys.: Condens. Matter* **2005**, *17*, 1415.
(31) Zhang, Z.; Sharma, P.; Borca, C. N.; Dowben, P. A.; Gruverman, A. *Appl. Phys. Lett.* **2010**, *97*, 243702.
(32) Kolpak, A. M.; Grinberg, I.; Rappe, A. M. *Phys. Rev. Lett.* **2007**, *98*, 166101.
(33) Inoue, Y.; Yoshioka, I.; Sato, K. *J. Phys. Chem.* **1984**, *88*, 1148.
(34) Yun, Y.; Pilet, N.; Schwarz, U. D.; Altman, E.I . *Surf. Sci.* **2009**, *603*, 3145.
(35) Burbure, N. V.; Salvador, P. A.; Rohrer, G. S. *Chem. Mater.* **2010**, *22*, 5823.
(36) Goniakowski, J.; Finocchi, F.; Noguera, C. *Rep. Prog. Phys.* **2008**, *71*, 016501.
(37) Lang, S. B. *Phys. Today* **2005**, *58*, 31.
(38) Whatmore, R. W. *Rep. Prog. Phys.* **1986**, *49*, 1335.
(39) Neidholdt, E. L.; Beauchamp, J. L. *Anal. Chem.* **2007**, *79*, 3945.
(40) Brownridge, J. D.; Shafroth, S. M. In *Trends in Lasers and Electro-Optics Research*; Arkin, W. T., Ed.; Nova Science Publishers: New York, 2006; pp 59−95.
(41) Rosenman, G.; Shur, D.; Krasik, Y. E.; Dunaevsky, A. *J. Appl. Phys.* **2000**, *88*, 6109.
(42) Tornow, W.; Shafroth, S. M.; Brownridge, J. D. *J. Appl. Phys.* **2008**, *104*, 034905.
(43) Fullem, T. Z.; Fazel, K. C.; Geuther, J. A.; Danon, Y. *Radiat. Res.* **2009**, *172*, 643.
(44) Wang, L. H.; Yuan, D. R.; Duan, X. L.; Wang, X. Q.; Yu, F. P. *Cryst. Res. Technol.* **2007**, *42*, 321.
(45) Powder Diffraction File 2, release 2001; Joint Committee on Powder Diffraction Standards−International Centre for Diffraction Data (JCPDS−ICDD), 2001.
(46) Inorganic Crystal Structure Database FINDIT, V1.1.4; FIZ Karlsruhe, Germany, 2008.
(47) Abrahams, S. C.; Reddy, J. M.; Bernstein, J. L. *J. Phys. Chem. Solids* **1966**, *27*, 997 (ICSD Col. Code 28294).
(48) Lundberg, M. *Acta Chem. Scand.* **1971**, *25*, 3337 (ICSD Col.Code 31930).
(49) Kato, K.; Tamura, S. *Acta Crystallogr. B* **1975**, *31*, 673 (ICSD Col. Code 1840).
(50) Ohgaki, M.; Tanaka, K.; Marumo, F. *Mineral. J.* **1989**, *14*, 373 (ICSD Col. Code 84226).
(51) Hummel, H. U.; Fackler, R.; Remmert, P. *Chem. Ber.* **1992**, *125*, 551 (ICSD Col. Code 66366).
(52) Tsirel'son, V. G.; Antipin, M. Y.; Gerr, R. G.; Ozerov, R. P.; Struchkov, Y. T. *Phys. Status Solidi A* **1985**, *87*, 425 (ICSD Col. Code 60419).
(53) TOPAS General Profile and Structure Analysis Software for Powder Diffraction Data, V2.0.; Bruker AXS GmbH: Karlsruhe, Germany, 2000.
(54) Cheary, R. W.; Coelho, A. A. *J. Appl. Crystallogr.* **1992**, *25*, 109.
(55) Levin, A. A. *RIET-ESD V1.0*; TU Dresden, Germany, 2005.
(56) Berar, J. F.; Lelann, P. *J. Appl. Crystallogr.* **1991**, *24*, 1.
(57) Lebel, C. P.; Ischiropoulos, H.; Bondy, S. C. *Chem. Res. Toxicol.* **1992**, *5*, 227.
(58) Bourree, L.; Thibaut, S.; Briffaud, A.; Rousset, N.; Eleouet, S.; Lajat, Y.; Patrice, T. *J. Photochem. Photobiol. B* **2002**, *67*, 23.
(59) Cathcart, R.; Schwiers, E.; Ames, B. N. *Anal. Biochem.* **1983**, *134*, 111.
(60) Wilkening, M.; Epp, V.; Feldhoff, A.; Heitjans, P. *J. Phys. Chem. C* **2008**, *112*, 9291.
(61) Madigan, M. T.; Martinko, J. M.; Parker, J. In *Brock Mikrobiologie*; Goebel, W., Ed.; Spektrum Akademischer Verlag: Heidelberg, 2001; p 165.
(62) Jiang, K.; Sun, T.-H.; Sun, L.-N.; Li, H.-B. *J. Environ. Sci.* **2006**, *18*, 1221.
(63) Nakamura, T.; Fujishiro, K.; Kubo, T.; Lida, M. *Ferroelectrics* **1994**, *155*, 207.

(64) Stancik, L. M.; Stancik, D. M.; Schmidt, B.; Barnhart, D. M.; Yoncheva, Y. N.; Slonczewski, J. L. *J. Bacteriol.* **2002**, *184*, 4246.
(65) Blake, D. M.; Maness, P.-C.; Huang, Z.; Wolfrum, E. J.; Huang, J.; Jacoby, W. *Sep. Purif. Rev.* **1999**, *28*, 1.
(66) Kalinin, S. V.; Johnson, C. Y.; Bonnell, D. A. *J. Appl. Phys.* **2002**, *91*, 3816.
(67) Buxton, G. V.; Greenstock, C. L.; Helman, W. P.; Ross, A. B. *J. Phys. Rev. Data* **1988**, *17*, 513.
(68) Legrini, O.; Oliveros, E.; Braun, A. M. *Chem. Rev. (Washington, DC, U. S.)* **1993**, *93*, 671.